Colloids and Surfaces B: Biointerfaces 181 (2019) 994–1003

Contents lists available at ScienceDirect

Colloids and Surfaces B: Biointerfaces

journal homepage: www.elsevier.com/locate/colsurfb

Production and characterization of a novel asymmetric 3D printed construct aimed for skin tissue regeneration

Sónia P. Miguel[a], Cátia S.D. Cabral[a], André F. Moreira[a], Ilídio J. Correia[a,b,*]

[a] CICS-UBI – Centro de Investigação em Ciências da Saúde, Universidade da Beira Interior, Av. Infante D. Henrique, 6200-506 Covilhã, Portugal
[b] CIEPQPF – Departamento de Engenharia Química, Universidade de Coimbra, Rua Silvio Lima, 3030-790 Coimbra, Portugal

ARTICLE INFO

Keywords:
Electrospinning
3D bioprinting
Asymmetric skin construct
Skin regeneration

ABSTRACT

Skin is a complex organ that act as the first protective barrier against any external threat. After an injury occurs, its structure and functions must be re-established as soon as possible. Among different available skin substitutes (epidermal, dermal and dermo-epidermal), none of them is fully capable of reproducing/re-establishing all the features and functions of native skin. Herein, a three-dimensional skin asymmetric construct (3D_SAC) was produced using electrospinning and 3D bioprinting techniques. A poly(caprolactone) and silk sericin blend was electrospun to produce a top layer aimed to mimic the epidermis features, *i.e.* to provide a protective barrier against dehydration and hazard agents. In turn, the dermis like layer was formed by printing layer-by-layer a chitosan/sodium alginate hydrogel. The results obtained in the *in vitro* assays revealed that the 3D_SAC display a morphology, porosity, mechanical properties, wettability, antimicrobial activity and a cytotoxic profile that grants their application as a skin substitute during the healing process.

1. Introduction

Skin is the body first line of defence, it provides protection against external harmful agents and plays a pivotal role in the maintenance of the body homeostasis [1,2]. Being the outermost organ of the body, it is susceptible to different types of injuries, such as acute (*e.g.*, surgical and traumatic wounds, abrasions and burns) and chronic wounds (*e.g.*, diabetic foot and pressure ulcers) [1]. Considering the wound size, extent, and depth, researchers have been developing different treatments, comprising various skin substitutes that are aimed to replace epidermis, dermis or both layers of the skin. Among them, the epidermal/dermal substitutes are the most advanced skin constructs [3]. Despite all the advancements attained so far, the currently available skin substitutes present several limitations that include poor tissue integration, due to inappropriate vascularization, deficient adhesion to the wound bed, scarring at the graft margins or incapacity to reproduce skin appendages [2,3].

To overcome these limitations, biomaterials, bioactive molecules, cells, and modern biomanufacturing techniques have been combined to develop new advanced skin constructs [2]. Among them, the asymmetric wound dressing have captured the attention of different researchers that have been employing various techniques, such as wet phase inversion, dry/wet, scCO2-assisted phase inversion and electrospinning, in their production process [4–7]. In 2010, Chen et al. combined the solvent evaporation, wet phase inversion, and organic-inorganic hybridization methods to produce a polyurethane asymmetric membrane loaded with nano-TiO_2. Their results revealed that the membrane' top layer avoided bacterial penetration, whereas the porous sublayer was able to absorb high amounts of exudate [8]. In turn, Morgado et al. used a $scCO_2$-assisted phase inversion technique to produce chitosan (CS)/polyvinyl alcohol asymmetric membranes loaded with ibuprofen, which by controlling the depressurization rate presented a thin top layer (thickness 15 μm) and a sponge bottom layer with uniform pore distribution [7]. Further, Miguel et al. produced a silk fibroin (SF) based asymmetric membrane using an electrospinning technique. The top layer was composed of SF and polycaprolactone (PCL), reproducing the waterproof ability of the epidermis, whereas the bottom layer constituted of SF, hyaluronic acid and loaded with thymol exhibited the porosity, wettability, antibacterial and antioxidant properties suitable for healing process [5]. Liang and their collaborators produced a silver nanoparticle/CS composite dressing displaying an asymmetric layered organization. To accomplish that, the authors prepared chitosan sponges loaded with silver nanoparticles through a lyophilization process. Then, one side of sponge was modified by a thin layer of stearic acid, which confers then waterproof and anti-adhesion properties to the external layer of the asymmetric membrane [9].

* Corresponding author at: CICS-UBI - Centro de Investigação em Ciências da Saúde, Universidade da Beira Interior, Avenida Infante D. Henrique, 6200-506, Covilhã Portugal.
E-mail address: icorreia@ubi.pt (I.J. Correia).

https://doi.org/10.1016/j.colsurfb.2019.06.063
Received 8 April 2019; Received in revised form 29 May 2019; Accepted 26 June 2019
Available online 28 June 2019
0927-7765/

Herein, a 3D_SAC was produced for the first time using both electrospinning and 3D printing techniques. The top layer was produced using the electrospinning since it allows the formation of fibers with a high surface-to-volume ratio and interconnected pores, which will allow cell penetration and nutrient exchange [10,11]. PCL and silk sericin (SS) were selected, for the first time, to produce the top layer due to their intrinsic properties. PCL is a synthetic polymer, widely known by its excellent mechanical resistance, biocompatibility and hydrophobicity. On the other side, SS is a biocompatible protein derived from the silk-worm cocoon with moisturizing capacity [11–14]. Further, SS can also act as antioxidant, bio-adhesive and bioactive agent, which is crucial for the healing process [15]. Moreover, Aramwith et al. described that SS could activate the collagen production in wounds and significantly increase the epithelialization rate [16]. Therefore, the combination of these two materials (PCL and SS) can reproduce the epidermis barrier like function.

On the other side, the 3D Bioprinting technique was used to replicate the dermis structure by promoting the sequential layer-by-layer deposition of both CS and sodium alginate (SA) [17,18]. The 3D printing technique allows the tailoring of the hydrogel' stiffness and geometry to precisely replicate the shape of the skin lesion [17–19]. Moreover, the 3D hydrogel possesses excellent intrinsic properties, like the high ability to absorb and retain the wound exudate, promoting the cell proliferation and migration, which are required for complete re-epithelization of the wound [20–23]. Moreover, this technique offers a great control on the geometry and interconnectivity of porosity as well as a higher mechanical stability [2]. On the other side, the bottom layer was produced with CS, which is a deacetylated derivative of chitin that exhibits several attractive properties (*e.g.* antimicrobial, biocompatible, biodegradable and haemostatic activity), which were already demonstrated in different wound dressings [6,11,21,24,25]. In fact, these properties triggered the production of wound dressings available in the market, such as Hidroki®, Patch®, Chitopack®, Tegasorb® and KytoCel® [26]. In turn, SA is a hydrophilic, biocompatible and biodegradable polymer, which is also widely used in different biomedical applications [27–31]. In skin regeneration area, the SA enhance the absorption of wound exudates, minimizing bacterial infections, reducing adverse allergic effects, and improving the healing process [32].

Overall, the data obtained in this study revealed that the produced 3D_SAC provides a dense top layer (electrospun membrane) that can act as protective barrier against microorganisms' infiltration and dehydration, while the porous bottom layer (3D printed hydrogel), affords a suitable structure and environment for cell migration and proliferation.

2. Methods

2.1. Production of the membrane (Polycaprolatone_Silk sericin)

The membrane, composed of polycaprolatone and silk sericin (**PCL_SS**), was produced using a conventional electrospinning apparatus, comprised of a high voltage power supply (Spellman CZE1000R, 0–30 kV, Spellman, USA), a precision syringe pump (KDS-100, Sigma-Aldrich, Portugal), a plastic syringe with a stainless-steel needle (21 Gauge), and an aluminium disk connected to a copper collector. For that purpose, a blend solution of PCL (9% w/v in TFE (80% v/v)) and SS (3% w/v in FA (98% v/v)) was prepared at 2:1 vol ratio. Afterwards, this solution was placed in the syringe and electrospun at a constant flow rate of 1.0 mL/h, using a working distance of 10–12 cm and an applied voltage of 28 kV, until the layer displayed a thickness quite similar to that exhibited by the epidermis layer of the human skin (0.05–1.5 mm).

2.2. Production of CS_SA hydrogels

In order to produce the hydrogel, a CS 8% (w/v) solution was prepared in AA (1% v/v)), and then mixed with SA (3% (w/v)) solution at 5:1 vol ratio. After that, the CS_SA solution was crosslinked with 5% $CaCl_2$ and completely homogenized with an X10/25 Ultra-turrax. Then, the blend was loaded into a syringe (10cc Luer Lock) and extruded using a Rapid Prototyping (Fab@Home) printer. The printed 3D model was designed using a CAD/CAM software (SolidWorks). The developed 3D model was composed of several layers angled at 90° with the underlying layer (0°–90°–180°), as shown in Fig. S1. After the 3D printing, the **CS_SA hydrogels** were crosslinked by immersion in 10% $CaCl_2$ (w/v) solution during 3 h. Then, the printed gels were washed with double-deionized and filtered water and the excess of water was absorbed with a filter paper.

The three-dimensional skin asymmetric construct (**3D_SAC**) was obtained by the electrospinning of the PCL_SS membrane on the top of the CS_SA hydrogel.

Afterwards, the mechanical, physicochemical and biological properties of 3D_SAC' layers were evaluated (please see the supporting information for further details).

3. Results and discussion

3.1. Characterization of the morphology of the produced layers

Artificial 3D structures have triggered the attention of researchers for tissue regeneration purposes. Matrices that closely mimic the extracellular matrix (ECM) favour cell proliferation and differentiation as well as allow nutrients, metabolites and soluble factors diffusion [33]. In this study, an asymmetric 3D construct composed of a dense and mechanical resistant top layer and a porous and bioactive bottom layer was produced using both electrospinning and 3D bioprinting techniques. The production of the nanofibrous top layer by electrospinning technique aimed to promote the cell-cell and cell-ECM interactions that occur at nano-scale level [10,34]. The high surface-to-volume ratio presented by the electrospun nanofibers favours the interaction between integrin receptors available on cell surface and nanofibrous membrane, triggering a cascade of four events: cell attachment, cell spreading, reorganization of actin cytoskeleton and formation of focal adhesions [22]. Further, this layer also works as a barrier against microorganism infiltration, as well as enables the drainage of the wound exudate and gaseous exchanges. Such properties are crucial to avoid the occurrence of skin infections and wound dehydration [5,11].

On the other hand, the 3D printed hydrogel provides a 3D structure with a porosity and microenvironment suitable for cell migration and proliferation [2,23]. Moreover, the hydrogel's hydrophilic polymer chains absorb high levels of exudate, keeping a moist environment at wound site whilst absorbing excessive exudate [21,22].

SEM analysis was performed to fully characterize both layers of the asymmetric skin construct (see Fig. 1 for further details). The PCL_SS top layer displayed a highly interconnected mesh composed of fibers with a mean diameter of 318.6 ± 93.75 nm, with a mean pore size of 629.45 ± 150.34 nm. In turn, the CS_SA hydrogel bottom layer presented macropores with a mean diameter of the 976.6 ± 141.69 µm. Moreover, the cross-sectional images of 3D_SAC revealed that the thickness of the top and bottom layers was 0.55 ± 0.16 mm and 1.59 ± 0.19 mm, respectively. Such results demonstrate that the combination of both techniques allowed the production of layers that reproduce the morphological features of the epidermis and dermis layers. The top layer nanofibers diameters are within the range of the collagen fibrils found at the ECM of human skin (50–500 nm) [10]. Further, the thickness of the top layer was tailored by optimizing the continuous deposition of the nanofibers until reaching a thickness similar to that exhibited by the epidermis layer (0.5–1.5 mm) [1]. In turn, the thickness of the bottom layer was controlled by the design of the 3D CAD model (Fig. S1), that allow to define the height of the 3D structures is within the range of the native dermis layer (0.6–3 mm), by controlling the number of printed layers [1]. Moreover, the existence of macropores in the bottom layer (CS_SA hydrogel) is essential for cell

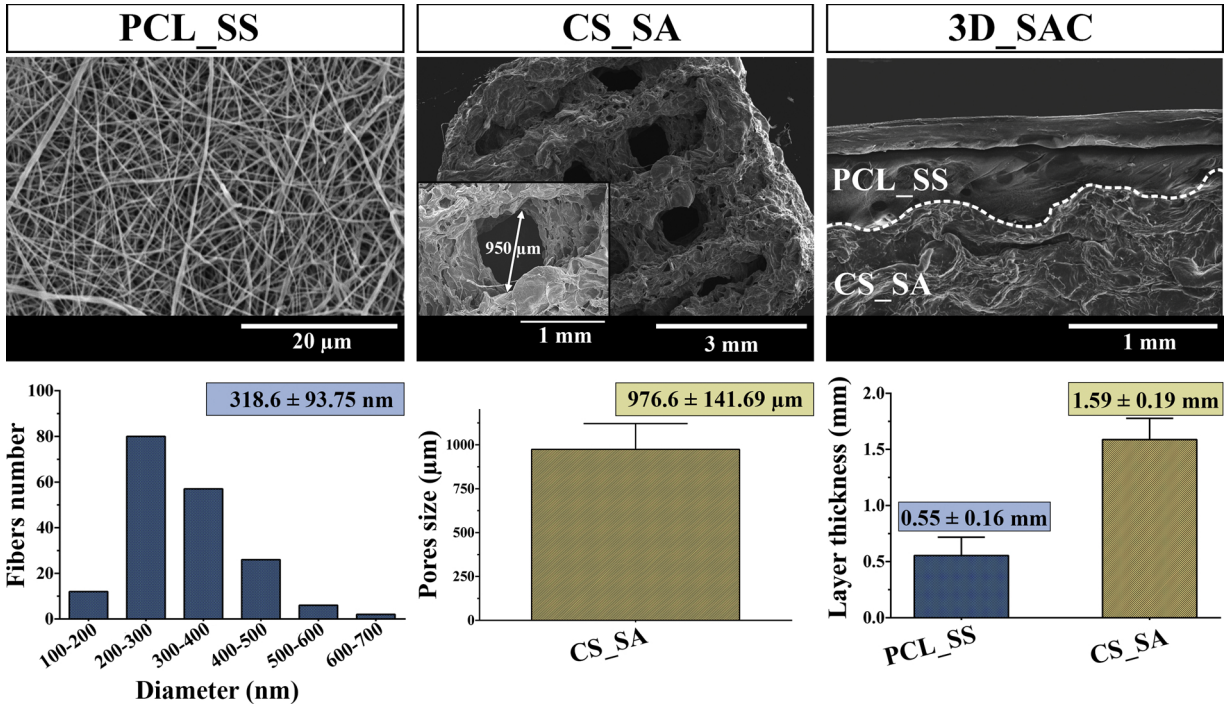

Fig. 1. Morphological analysis of both layers of the 3D_SAC. SEM images of the top (PCL_SS), bottom (CS_SA) layer and cross-section of the 3D_SAC. Analysis of the top layer fiber' size distribution, bottom layer mean pore size and layer thickness.

nutrition and proliferation as well as for formation of new tissues and nutrients/oxygen diffusion into the wound site [21,23]. Indeed, according to Loh and coworkers, the pore size and total porosity are parameters that have a direct impact on cell viability and proliferation, and consequently on the healing process [35].

3.2. Attenuated total reflectance-Fourier transform infrared spectroscopic analysis

The chemical composition of the produced membrane and hydrogel was characterized by FTIR analysis. The spectrum of the top layer (Fig. 2A) displays the characteristic peaks of SS at 1631 cm^{-1} (Amide I, which arises from the C=O stretching vibrations of the peptide linkages), at 1527 cm^{-1} (Amide II, that derives from N–H bending and the C–N stretching vibration), at 1239 cm^{-1}(Amide III, represents primarily the C–N stretching vibration linked to N–H bending vibration). Furthermore, the presence of the amide I peak at 1631 cm^{-1} also show that the SS possess a β-sheet conformation [36,37]. Such data is in accordance with the work published by Tsukada, which reported that the SS recovered by this extraction protocol (hot water) mainly presents β-sheet structures, due to the lyophilization process, with 10% of α-helice conformation [38]. In addition, the PCL_SS spectrum also presents the PCL characteristic peaks at 2942 cm^{-1} (asymmetric CH_2 stretching), 1724 cm^{-1} (carbonyl stretching), 1293 cm^{-1} (C–O and C–C stretching), 1239 cm^{-1} (asymmetric C–O–C stretching) and 1139 cm^{-1} (symmetric C–O–C stretching) [5,11,39].

On the other hand, the characteristic peaks of the bottom layer's components are presented in Fig. 2B. The peaks of CS appear at 3293 cm^{-1} (–OH stretch), 2871 cm^{-1} (aliphatic C–H stretch), 1648 cm^{-1} (NH_2 stretch), 1374 cm^{-1} (–C–O stretching of the primary alcohol group) and at 1026 cm^{-1} (C–O–C glycosidic bond) [11,12,17]. Further, the peaks of the SA are presented between 3000-3700 cm^{-1} (–OH stretch of water and –OH groups of the G and M units of alginate) and at 1597 cm^{-1} and 1406 cm^{-1} (C=O stretching vibration of the carboxylic group of alginate) [29].

3.3. Evaluation of the 3D_SAC mechanical properties

Wound dressings must display mechanical properties that allow them provide mechanical support that is required to protect the wound

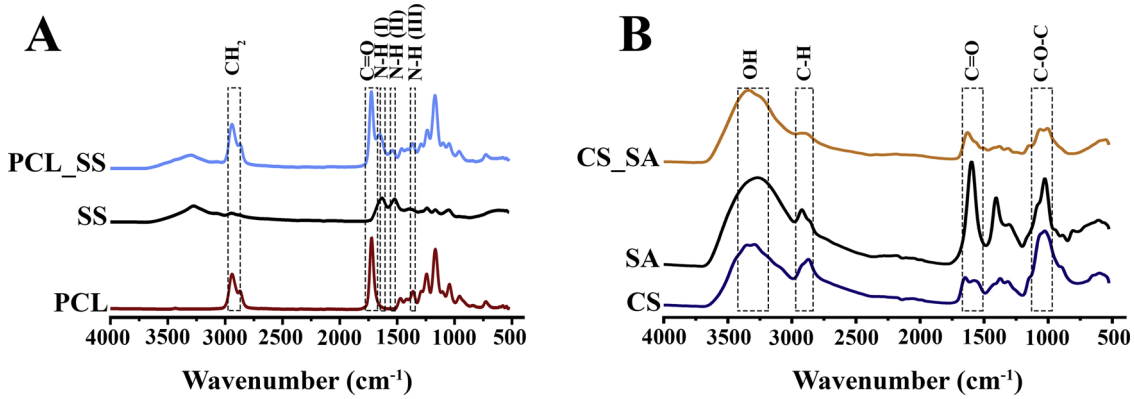

Fig. 2. ATR-FTIR analysis of the top (PCL_SS membrane) (A) and bottom (CS_SA hydrogel) (B) layers and their respective raw materials.

from external threats [4,40]. Herein, the mechanical properties of the top layer were evaluated through the tensile assays, whereas the bottom layer' mechanical performance was characterized using a compressive assay. In relation to the PCL_SS top layer, the obtained values for tensile strength, Young's modulus, and elongation at break, in wet state, were 34.92 ± 7.39 MPa, 27.92 ± 8.09 MPa, and 155.37 ± 5.71%, respectively. On the other side, the bottom layer (CS_SA hydrogel) displayed a compressive strength and Young's modulus of 0.16 ± 0.05 MPa and 0.05 ± 0.01 MPa, respectively. These results confirm the excellent mechanical properties of the top layer, that present similar tensile strengths (5–30 MPa), Young modulus (4.6–20 MPa), and elongation at break (35–115%) values to those displayed by the native skin [5,7,11]. Such mechanical performance can be attributed to the PCL, a synthetic polymer well known by its mechanical strength [41]. In turn, the CS_SA hydrogel presented a lower mechanical performance, which can be attributed to the higher porosity of this layer (Fig. 1 and 3A). In fact, the production of porous scaffolds with a best compromise between porosity and mechanical strength is still one the major challenges faced by the researchers [42]. Further, the hydrogel was produced only with natural polymers (CS and SA), which are widely recognized by their weak mechanical properties [43,44]. However, the CS_SA hydrogel exhibited compressive strength values quite similar to the native skin (0.2 −7 MPa). Additionally, these results are in accordance with compressive strength and Young modulus values (0.46 ± 0.22 MPa and 8.16 ± 1.75 MPa, respectively) reported in literature by Liu et al. for CS_alginate hybrid scaffolds [45]. The mechanical properties exhibited by the produced layers emphasized their suitability for being applied during the healing process.

3.4. Determination of the layers' porosity and skin construct

Biomaterials' porosity is a key parameter for their application in tissue engineering. An interconnected pore structure and high porosity are essential features to ensure cellular penetration and the adequate nutrients diffusion within the construct and to ECM produced by these cells [33,46]. Herein, the total porosity was determined using a liquid displacement method [5,11]. The obtained results revealed that the PCL_SS membrane and the CS_SA hydrogel have a porosity of 56.66 ± 2.47% and 99.08 ± 5.31% respectively, whereas the 3D_SAC display a total porosity of 79.13 ± 2.55%, a value comprehended between the individual layers (Fig. 3A). Such results are in accordance with the morphological variations observed in SEM images (Fig. 1). In fact, the electrospun top membrane provides a nano-scale and a polymeric dense network composed by the interconnected fibers, that display a low porosity, which avoids microorganisms invasion [47]. Further, the low porosity displayed by the top layer is crucial to this layer to act as a protective barrier [5]. On the other hand, the 3D printed hydrogel exhibits a highly porous polymeric structure with macropores that are compatible with cell migration and proliferation, as well as absorption of the excess of the exudate from the wound site. Additionally, the CS_SA hydrogel high porosity is in agreement with those reported in the literature for CS hydrogels, where the porosity values range from 75%–85% [48]. Further, the CS_SA hydrogel exhibited a porosity value similar to those displayed by the acellular dermal matrix (68.3 ± 5.8%) [49].

However, it is worth to notice that the biomaterials porosity has a direct impact on the mechanical properties of the 3D networks, *i.e.*, the biomaterials structural stability is impaired by an increased porosity. Indeed, Venugopal et al. evaluated this influence on the production of PCL/nanohydroxyapatite/collagen nanofibers. Their results revealed that an increase in the pore size from 2 to 15 μm to 5–50 μm, promoted an augment on porosity from 72.3% to 89.7% and a decrease on the tensile strength from 2.72 MPa to 1.28 MPa [50]. So, in this work, the combination of the 3D hydrogel with the electrospun membrane enabled the production of a 3D _SAC displaying a porosity within the preferred range (60–90%), which is fundamental to promote cell accommodation and migration [24].

3.5. Characterization of the swelling profile of the layers and skin construct

The healing process was associated with the production of wound exudate, which is a complex mixture of water, soluble inflammatory mediators, proteases, growth factors, and electrolytes [39]. However, an abnormal production of wound exudate (resultant from the prolonged inflammation stage, wound bed infection, and chronic healing) leads to tissue maceration and excoriation in the periwound region. Further, an excessive amount of exudate impairs the cellular migration towards to the wound bed, avoiding the proper tissue replacement and hence extending the healing period [45]. Herein, the capacity of the individual layers and 3D_SAC to absorb the wound exudate was characterized by evaluating their swelling profile (Fig. 3B). The results clearly demonstrate that the CS_SA hydrogel layer presents the higher swelling ratio (≈ 43) after 10 h of immersion, whereas the PCL_SS membrane and 3D_SAC only reach their maximum swelling ratio (≈ 29 and ≈30, respectively) after 18 h of incubation.

The higher swelling ratio of the hydrogel layer can be explained by the presence of hydrophilic groups (amine, hydroxyl, and carboxyl) on CS and SA backbones that can be easily hydrated [11,19,31]. As previously described by Raja and Fathima, the -NH_2 and −OH groups located at each *N*-acetyl-glucosamine and glucosamine residues of the CS and SA backbone interact with water molecules through hydrogen bonding [22]. However, the continuous swelling cause the loss of the mechanical integrity and compressive stress to surrounding tissue [51]. Herein, the greater swelling ratio of hydrogel was controlled through the presence of the PCL_SS membrane, as demonstrated by the data obtained for 3D_SAC. Further, the 3D_SAC swelling profile is compatible with the adsorption of the wound exudate, which combined with the capacity to allow gaseous exchanges (*e.g.* water vapor transmission) should allow the maintenance of an environment moisture in values that promote the healing process.

3.6. Evaluation of the degradation profile of the layers and skin construct

Most of the commercially available wound dressings are non-degradable, requiring their replacement/removal and consequently favouring the scar tissue formation and leading to an increased risk of bacterial contamination [52]. Due to that, the development of biodegradable structures that display a degradation profile compatible with the rate of skin regeneration is a key requirement of wound dressings [12,40]. Herein, the degradation profiles of the individual layers and asymmetric skin construct were evaluated using lysozyme, an enzyme found in human serum that can degrade CS-based materials [53]. After 7 days of incubation in Tris buffer solution (containing lysozyme), the CS_SA hydrogel presented the highest weight loss (65.44 ± 6.93%), whereas the PCL_SS membrane displayed the lowest one (17.33 ± 6.81%), and the 3D_SAC had an intermediate weight loss of 33.39 ± 6.81% (Fig. 3C). The improved stability of PCL_SS membrane can be attributed to the PCL, an aliphatic polyester that suffer low degradation through hydrolysis or by the action of metalloproteinases [5,41]. In turn, the SS present on the top layer is mainly decomposed through hydrolytic degradation processes. Such, is explained by the highly hydrophilic character of SS side chains (hydroxyl, carboxyl, and amino groups) [46]. In opposition, the accelerated degradation prolife of the 3D hydrogel can be justified by i) the CS degradation mediated by the lysozyme hydrolyzation of the *N*-acetyl glucosamines groups [53]; ii) the SA disintegration by gradual replacement of calcium by sodium ions present in the medium; and iii) the weak ionic interaction established between the amino groups of CS and the carboxyl groups of SA [45]. Further, the SA can also become depolymerized through the spontaneous alkaline elimination of its glyosidic linkages that occur *in vivo* [19,31].

Herein, the strong entanglement between the two layers (PCL_SS

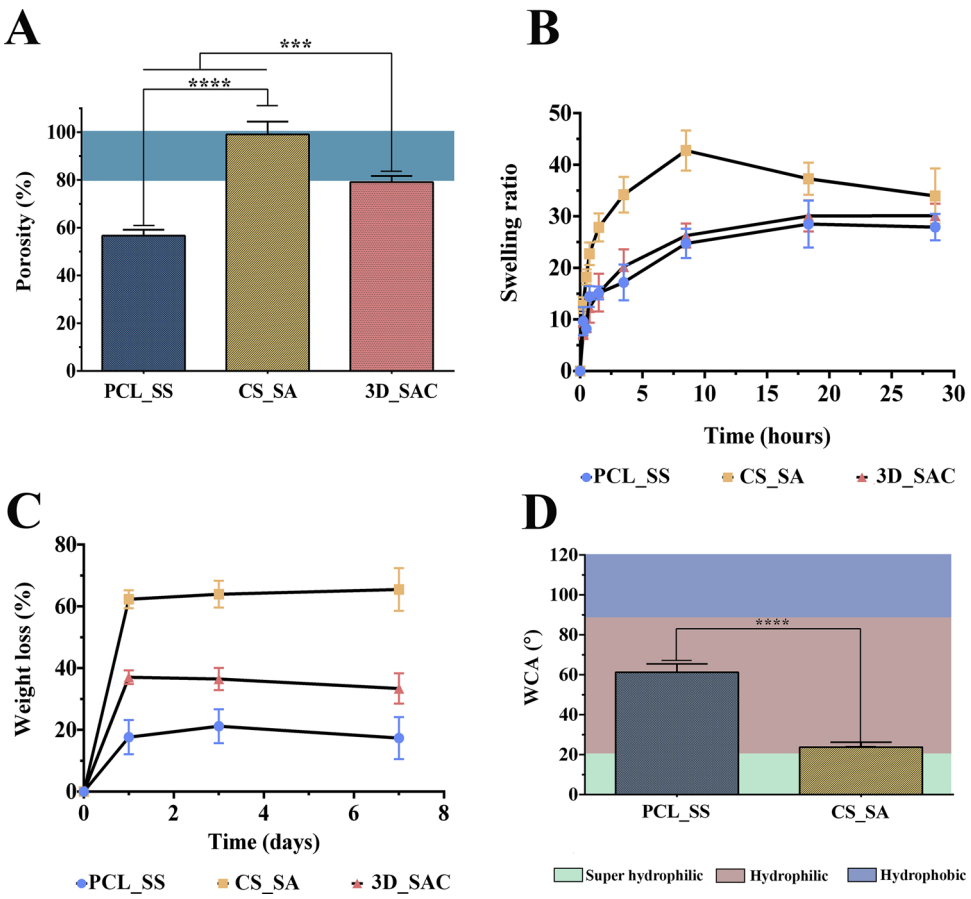

Fig. 3. Evaluation of the total porosity (A), swelling profile (B), weight loss profile (C) and the wettability of the PCL membrane, CS_SA gel, and 3D_SAC (D). Data are presented as the mean ± standard deviation, n = 5, ***p < 0.001, ****p < 0.0001.

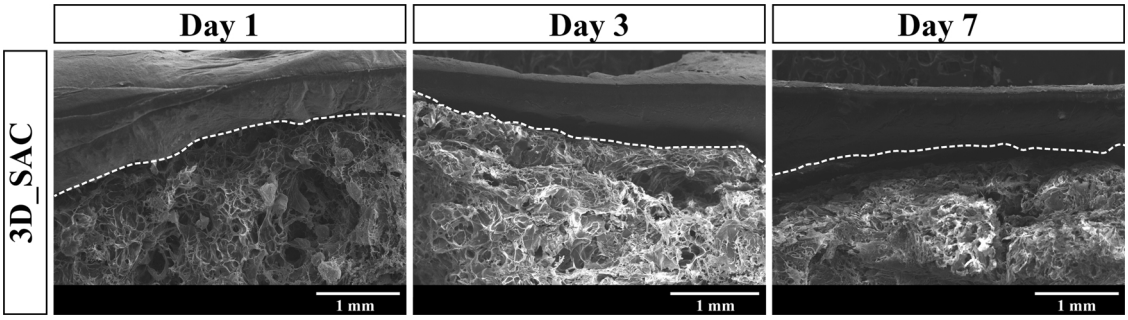

Fig. 4. SEM images of the 3D_SAC cross-sections after their incubation in Tris-buffered saline solution (pH 5) for 1, 3, and 7 days.

membrane and CS_SA hydrogel) allowed the production of the 3D_SAC with a weight loss value comprehended between the weight losses displayed by the individual layers. In Fig. 4, the cross-section of the 3D_SAC can be visualized after 1, 3 and 7 days of incubation. These images demonstrate that despite the decrease in the bottom and top layers density (more perceptible in bottom layer), they remain attached during at least 7 days.

3.7. Determination of the WVTR of skin asymmetric construct

The maintenance of a moist environment at the wound bed is crucial for an effective healing to occur. In fact, a moist environment avoids patient dehydration as well as enhances the angiogenesis and the collagen synthesis [20]. The wound dressings' water evaporation transmission rate (WVTR) is also an important feature to maintain a moist environment at wound site, favouring the cell proliferation. In fact, the 3D_SAC presented a WVTR value of 1737.85 ± 192.12 mL/m^2/day, which is similar to those found on other asymmetric membranes previously produced (*e.g.* asymmetric PCL/CS_AV_PEO membrane (1252.35 ± 21.22 g/m^2/day) [11], PCL_HA/ CS_Zein electrospun bilayer membrane (1762.91 ± 187.50 g/m^2/day) [12] and Silk Fibroin based asymmetric membrane (2070.62 ± 102.52 mL/m^2/day) [5]). Further, the 3D_SAC capacity to provide a suitable moisture environment is superior to that displayed by commercial wound dressings (*e.g.* 285 ± 8 g/m^2/day for Comfeel (Coloplast A/S); 394 ± 12 g/m^2/day for Bioclusive (Johnson-Johnson); and 792 ± 32 g/m^2/day for Op Site (Smith & Nephew) [54]). In addition, according to the literature, the wound dressings with WVTR values comprehended between 2000 and 2500 mL/m^2/day are more prone to maintain a favourable environment for cell proliferation and water vapor exchanges [7,8,44].

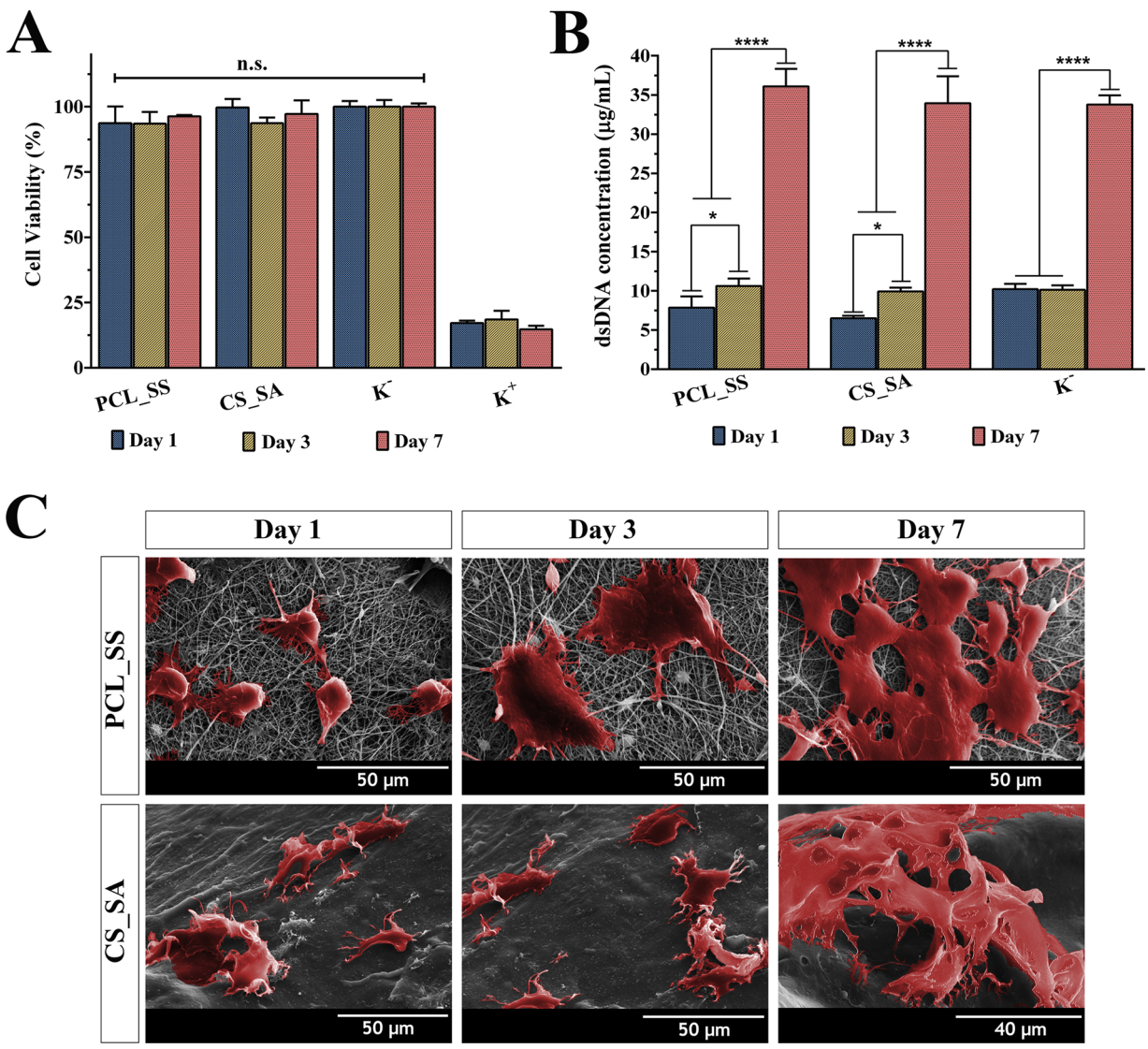

Fig. 5. Characterization of the cytotoxic profile of the layers. Analysis of the NHDF cell viability (A) and dsDNA content (B) after 1, 3, and 7 days of incubation. Representative pseudo-coloured SEM images of NHDF cells seeded at the surface of the top and bottom layers of skin asymmetric construct after 1, 3, and 7 days (C). Data are presented as the mean ± standard deviation, n = 5, ****$p < 0.0001$; the groups assigned with n.s. were not statistically significant.

3.8. Characterization of the layers' wettability

The biological response to the biomaterial implantation is closely related to the cellular interaction at the biomaterials' surface [55]. Among the different surface features, the surface wettability has a direct impact on the cell adhesion process [56]. In this way, the wound dressing wettability was also evaluated through the determination of the water contact angles (WCA) at the layers' surface (Fig. 3D). The PCL_SS membrane presented a WCA value of 61.27 ± 4.15°, indicating a moderate hydrophilic character (40° < WCA < 70°) [11,56]. Such result can be explained by the presence of highly hydrophilic hydroxyl, carboxyl, and amino groups on SS backbone [13,14], that counterbalance the hydrophobicity of the PCL aliphatic polyesters chains [11,41]. On the other side, the bottom layer of the asymmetric skin construct (CS_SA hydrogel) exhibited a WCA value of 23.75 ± 2.46°, revealing a superhydrophilic character (WCA ≈ 20°). Such result can be explained by the high percentage of hydrophilic groups (*e.g.* amine, hydroxyl, and carboxy) on CS and SA backbones [45]. According to the literature, cell adhesion-mediating ECM proteins (*e.g.* vitronectin, fibronectin, collagen or laminin) are more prone to become adsorbed on hydrophilic surfaces [55,56].

3.9. Characterization of the layers' biological properties of the asymmetric skin construct

The cytotoxic profile of asymmetric skin construct was evaluated through the incubation of the PCL_SS membrane and CS_SA hydrogel in contact with NHDF, which were used as model cells. Fibroblasts were selected to perform these assays, since they are involved in the production of ECM components (collagen and fibronectin), cytokines and growth factors, which are essential for the reestablishment of the damaged tissue' structure. Optical microscopic images of NHDF cells seeded in contact with the layers after 1, 3 and 7 days are presented in Fig. S2. Such images revealed that the NHDF cells do not suffer any morphological variation when seeded in contact with samples. Cells display a similar morphology to that of the negative control (cells seeded only in contact with culture medium). Moreover, the cytotoxic profile of the 3D_SAC' layers was also evaluated through the MTS assay over 1, 3 and 7 days (Fig. 5A). Such results show that both layers did not elicit any cytotoxic effect on NHDFs, over the 7 days. Further, the dsDNA quantification results (Fig. 5B) corroborated the data obtained in the MTS assay, thus revealing that the NHDFs remained viable and proliferated in contact with the produced layers for 7 days.

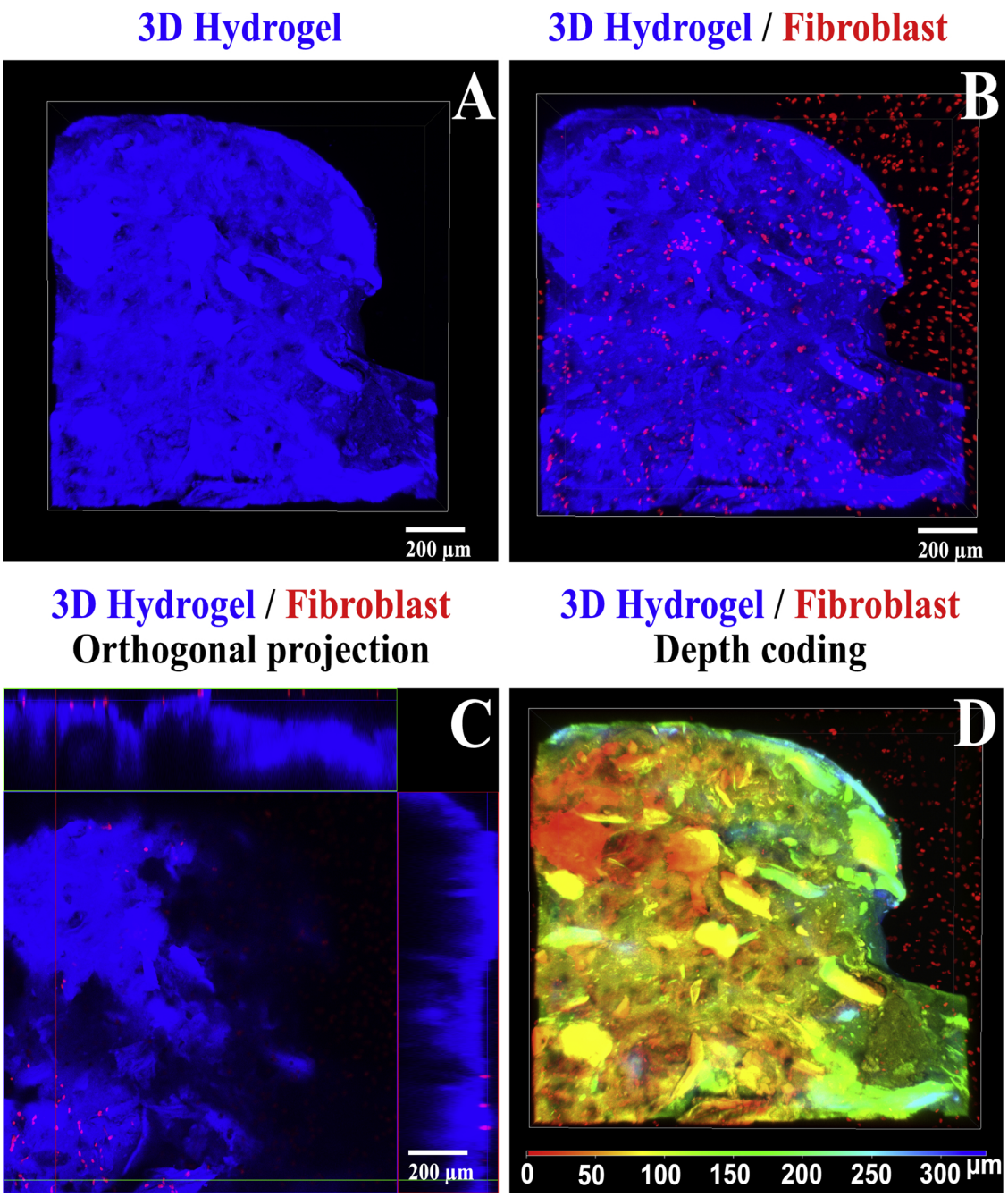

Fig. 6. CLSM images of the cellular within CS_SA hydrogel. 3D reconstruction images (A and B) and orthogonal projection (C) of the cells seeded in contact with the hydrogel. Depth colour coding CLSM image of the hydrogel (D).

Apart from the biocompatibility, a wound dressing must also favour cell attachment, growth, and proliferation. The SEM images presented in Fig. 5C show that the surface topography of both layers was able to promote the cell adhesion and proliferation. Indeed, after 7 days, the cells presented the typical fibroblastic morphology, exhibiting a smooth arrangement, and established interconnections between each other, forming a continuous cell layer. Additionally, the number of NHDF cells adhered on the layers' surface increased overtime, which further supports membranes biocompatibility.

Live/dead assays were also performed to further characterize the 3D_SAC' layers cytocompatibility through the staining of live and dead cells with calcein and propidium iodide, respectively [5,39]. The CLSM images (Fig. S3) clearly show that the cells remained viable (green channel) and presented an uniform cell distribution throughout the both layers of the 3D_SAC. Such results can be explained by the presence of SS and CS in the composition of the top and bottom layers, respectively. In fact, Tsubouchi et al. found that SS enhanced the attachment of primary cultured human skin fibroblasts on petri dishes coated with SS [57]. SS besides displaying a hydrophilic character also possess various amino acid on its backbone (*e.g.* serine, glycine, and aspartic acid) that are known for their capability to promote cell adhesion, spreading and proliferation, and thereby improving the healing process [16].

On the other hand, in the bottom layer, the interaction of the cell membrane glycosaminoglycans with the amine groups of CS present in CS_SA hydrogel promotes cell adhesion [21,58]. Moreover, the CS provides a 3D network that promotes cell proliferation and tissue organization [59].

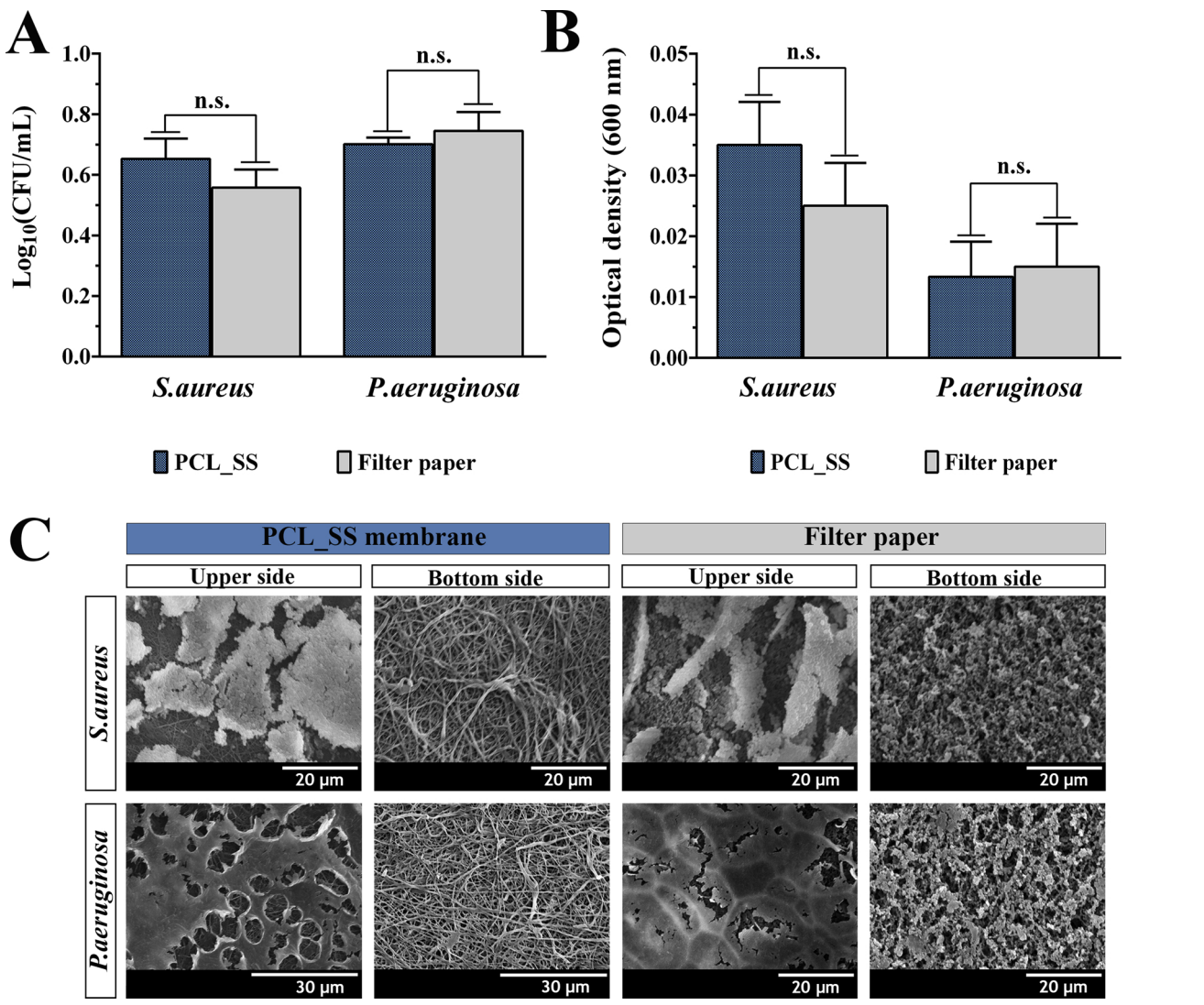

Fig. 7. Evaluation of the bacterial infiltration through PCL_SS membrane and filter paper (control group). Determination of the number of CFU of *S. aureus* and *P. aeruginosa* that crossed the PCL_SS membrane or filter paper, after 24 h (A). Optical density of medium samples recovered from the lower chamber of the transwell system (B). Data are presented as the mean ± standard deviation, n = 5, n.s. = non-significant. SEM images of the microorganisms (*S. aureus* and *P. aeruginosa*) that adhered to the upper or lower side of the PCL_SS membrane and filter paper are presented in (C).

Fibroblast cells migration and proliferation within CS_SA hydrogel (bottom layer) was also characterized through confocal microscopy analysis (Fig. 6). The CLSM images presented in Fig. 6B show that the cells were able to migrate into the interior of CS_SA hydrogel. Cellular internalization is further noticeable in the orthogonal projection shown in Fig. 6C. In addition, the depth colour coding images also confirm that the NHDF cells migrated into hydrogels interior through their pores. Such results confirm that the porous structure of the printed CS_SA hydrogel was suitable for the accommodation and proliferation of NHDFs, as well as to allow an effective nutrient supply and metabolic waste removal, processes that are essential for an effective cell growth and subsequently skin regeneration occur [21,60]. When the NHDFs reach the wound site, they start to produce and secrete ECM proteins (essentially collagen type III) and growth factors (*e.g.*, Transforming Growth Factor-1 (TGF-1), Fibroblast Growth Factor (FGF) and Vascular Endothelial Growth Factor (VEGF)) that play pivotal roles in the restoration of the injured skin' structure [12]. Together, these results demonstrate that the 3D_SAC mimic the native human skin structure and promote the healing process.

3.10. Evaluation of the antimicrobial properties of the produced layers

A wound is highly susceptible to bacterial contamination, leading to the infection that can often impair the healing process, leading to high rates of morbidity and mortality [39]. Once bacteria adhered to wound surface, a cascade of events occur, leading to the formation of biofilms [26]. In this way, it is crucial to develop wound dressings showing antimicrobial activity that are capable of inhibiting bacteria growth. In this study, the antimicrobial properties of the produced layers of 3D_SAC were characterized using *S.aureus* and *P.aeruginosa*, as models of gram-positive and gram-negative bacteria, respectively. These bacterial strains were selected since they are the most common pathogen found in skin infections [5,26].

The membrane top layer (PCL_SS), which will be in direct contact with the external environment, was conceived to avoid microbial invasion of the wound site. The results presented in Fig. 7A and B show that the top layer of 3D_SAC, acts as protective barrier, hampering the infiltration of the both bacteria. Further, it is noticeable that there is no significant difference with the control group, a filter paper (pore size of

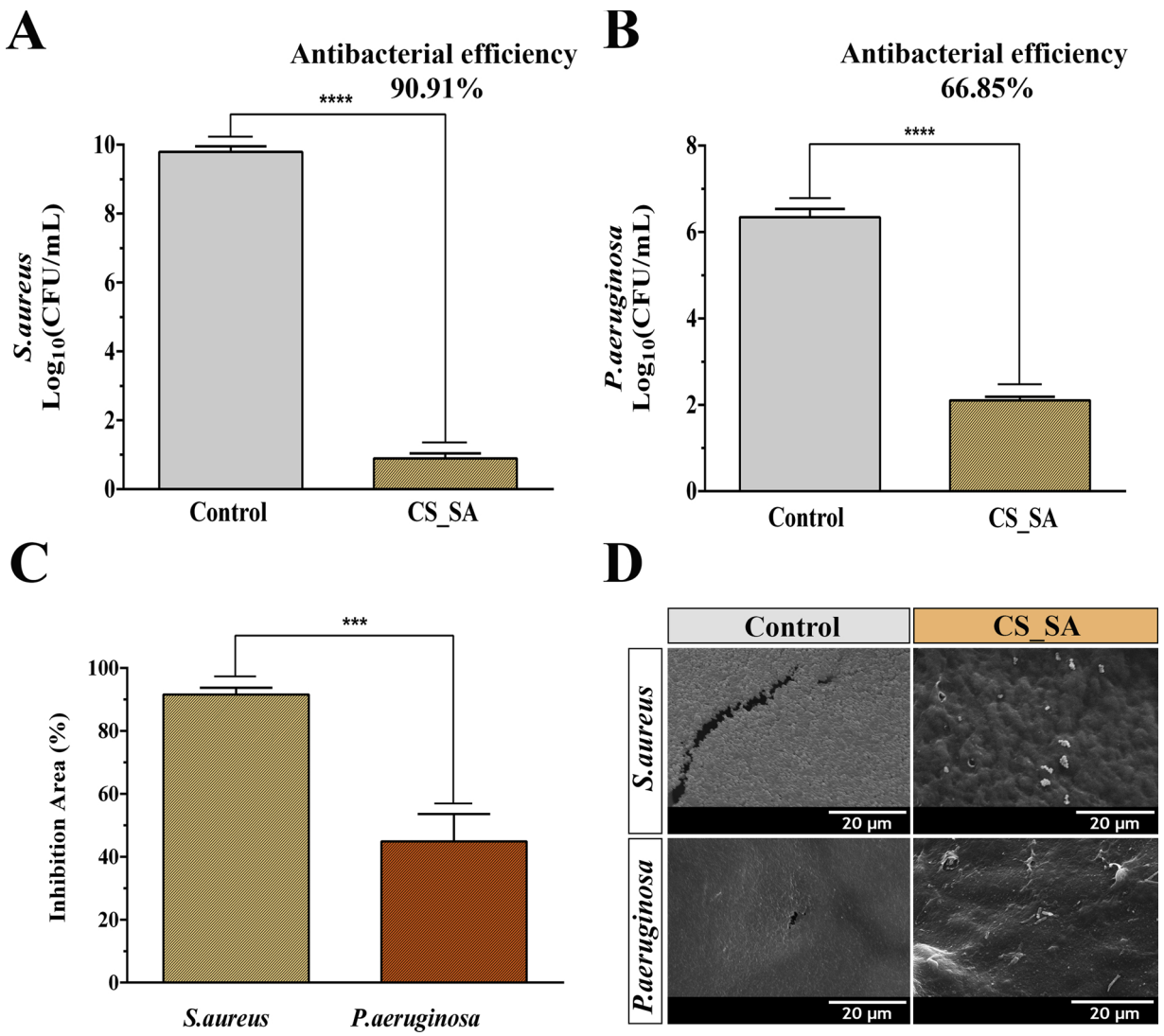

Fig. 8. Evaluation of the CS_SA layer antibacterial efficiency against *S.aureus* (A) and *P.aeruginosa* (B). Data are presented as the mean ± standard deviation, n = 5, ***p < 0.001, ****p < 0.0001. Determination of the inhibition area displayed by the bottom layer, when placed in contact with both bacterial models (C). SEM images of control and CS_SA hydrogel incubated with *S. aureus* and *P. aeruginosa* (D).

0.22 µm, which is usually used for sterilization purposes). In addition, the SEM images (Fig. 7C) revealed that despite some bacteria can adhere to the upper side of the top layer, no bacteria penetration to the bottom side of the nanofibrous layer occurred. Such results highlighted the capacity of the top layer to act as a barrier, due to its low porosity, that hampers the microorganisms' colonization of the wound site [4]. Further, despite of few works reporting the antibacterial properties of SS, different authors proposed that the bactericidal activity presented by this protein results from the interaction of the protonated amino groups of SS with the negatively charged groups available on the bacterial cell wall (surface components like lipopolysaccharides and proteoglycans) [25,36]. Moreover, SS with low molecular weight could penetrate the bacterial cells directly resulting in the loss of the cell's integrity, as already reported in works performed by Doakhan et al. [61], and Zhao et al. [25].

Additionally, the bottom layer (CS_SA hydrogel) capacity to provide an aseptic environment to the wound was also evaluated. To accomplish that, hydrogels were incubated over 24 h with bacteria models (*S.aureus* and *P.aeruginosa*) and then the number of colonies formed were counted. The results revealed that the CS_SA hydrogel exhibited an inhibitory effect on bacterial growth of 90.91% and 66.85% for *S.aureus* and *P.aeruginosa* (Fig. 8A and B), respectively. To further assess the antibacterial activity of the bottom layer, the modified Kirby-Bauer assay was also performed. The results corroborated the antibacterial activity of the bottom layer, since an inhibition area of ≈ 92% and ≈ 45% was determined for *S.aureus* and *P.aeruginosa*, respectively (Fig. 8C). Further, no biofilm formation was noticed at the surface of the CS_SA layer, when it was incubated with the microorganisms (Fig. 8D). In contrast, biofilm formation occurred in the control samples, where bacteria were seeded on contact with agar plate (without the CS_SA hydrogel). The bactericidal activity of the 3D_SAC bottom layer can be explained by the presence of CS in the hydrogels' formulation, which is widely described in the literature as material with antimicrobial properties. For example, Antunes et al. produced CS-based wound dressings and they obtained an inhibitory effect of ≈ 50% and ≈ 16.5% for *E.coli* and *S.aureus* [24]. In a similar way, Nguyen and their collaborators produced co-axial PLA/CS nanofibers and they obtained an antibacterial efficiency between 100% and 52% for *E.coli* [62]. Different mechanisms have been proposed to explain the antimicrobial activity of CS. Although, the most one, purposes that the electrostatic interactions occurring between the positively charged amine groups of CS and the negatively charged groups available on the bacterial cell wall are responsible for CS bactericidal effect [26,63]. Such interactions will increase the cell wall permeability, and

consequently, allow the leakage of the intracellular constituents that lead to the disruption of the ionic gradients found within the bacteria. Further, the CS can also promote the formation of a polymeric envelope around the bacteria, leading to the inhibition of cell exchanges and nutrients absorption [4,21,26,63].

It is worth to notice that the antibacterial effect of CS is influenced by the structure and composition of the bacterial cell wall. In fact, the data obtained revealed that the CS_SA hydrogel presented a more pronounced antibacterial effect towards *S.aureus* (gram-positive bacteria), as shown in Fig. 8. Similar observations have also been reported by other researchers in the literature [17,64]. Gram-negative bacteria (*P.aeruginosa*) cell wall is more complex and thicker, possessing an outer membrane composed of lipopolysaccharides and proteins. As a phospholipid bilayer, the lipid portion of the outer membrane is largely impermeable to charged macromolecules, such as CS [64].

4. Conclusions

The asymmetric membranes potential to be used in wound dressing applications has been recognized in different reports available in the literature. In fact, the reproduction of native skin' structure allows them to mimic the epidermis and dermis' functions, avoiding the microbial invasion and simultaneously, promoting the cell adhesion and proliferation. Despite the several dermo-epidermal skin substitutes available in the market, none of them is able to fully capable of mimicking the structure and functions of the skin layers, while promoting the healing process.

In this work, it was reported for the first time, the production of a 3D asymmetric skin construct combining the electrospinning and 3D bioprinting technology. The epidermis layer was mimicked through the production of a dense and interconnected polymeric nanofibrous membrane (PCL_SS), which act as physical protective barrier to the wound site. The top layer was able to avoid the microorganisms' infiltration and present excellent mechanical properties (tensile strength, young modulus, and elongation at break), quite similar to those displayed by native human skin. On the other side, the bottom layer (CS_SA hydrogel) obtained by using a 3D Bioprinting technique exhibited an adequate porosity, wettability and biological properties for supporting cell adhesion, migration, and proliferation, as well as, inhibit the *S.aureus* and *P.aeruginosa* growth. In the near future, the incorporation of bioactive molecules (*e.g.* growth factors, proteins, vitamins, anti-inflammatory drugs, and cells) into PCL_SS membrane and CS_SA hydrogel can be performed for improving the 3D asymmetric skin construct' performance on the wound healing process. Furthermore, *in vivo* assays may be pursued to fully depict the therapeutic potential of the 3D_SAC for enhancing the skin regeneration, emphasizing the suitability of this asymmetric 3D skin construct for the treatment of the skin injuries, which affect millions of patients worldwide.

Acknowledgments

The authors would like to acknowledge Abílio Silva for the help in the mechanical assays. Financial support was provided by FEDER funds through the POCI —COMPETE 2020 —Operational Programme Competitiveness and Internationalization in Axis I —Strengthening research, technological development, and innovation (Project POCI-01-0145- FEDER-007491) and National Funds by FCT —Foundation for Science and Technology (Project UID/Multi/00709/2013). The funding from CENTRO-01-0145-FEDER-028989 and POCI-01-0145-FEDER-031462 is also acknowledged. Sónia P. Miguel and André F. Moreira acknowledges their Ph.D. fellowships from FCT (SFRH/BD/109563/2015 and SFRH/BD/109482/2015, respectively).

Appendix A. Supplementary data

Supplementary material related to this article can be found, in the online version, at doi:https://doi.org/10.1016/j.colsurfb.2019.06.063.

References

[1] P.A. Kolarsick, et al., J. Dermatol. Nurses Assoc. 3 (2011) 203–213.
[2] S. Vijayavenkataraman, et al., Biofabrication 8 (2016) 032001.
[3] P.I. Morgado, et al., J. Membr. Sci. 490 (2015) 139–151.
[4] S.P. Miguel, et al., Int. J. Biol. Macromol. 127 (2019) 460–475.
[5] S.P. Miguel, et al., Int. J. Biol. Macromol. 121 (2019) 524–535.
[6] F.-L. Mi, et al., J. Membr. Sci. 212 (2003) 237–254.
[7] P.I. Morgado, et al., J. Membr. Sci. 469 (2014) 262–271.
[8] Y. Chen, et al., J. Appl. Polym. Sci. 119 (2011) 1532–1541.
[9] D. Liang, et al., ACS Appl. Mater. Interfaces 8 (2016) 3958–3968.
[10] S.P. Miguel, et al., Colloids Surf. B Biointerfaces 169 (2018) 60–71.
[11] S.P. Miguel, et al., Polymers 9 (2017) 183.
[12] D.R. Figueira, et al., Int. J. Biol. Macromol. 93 (2016) 1100–1110.
[13] Y.-Q. Zhang, Biotechnol. Adv. 20 (2002) 91–100.
[14] L. Lamboni, et al., Biotechnol. Adv. 33 (2015) 1855–1867.
[15] L. Cuttle, et al., Burns 32 (2006) 806–820.
[16] P. Aramwit, et al., Int. J. Mol. Sci. 11 (2010) 2200–2211.
[17] C.S. Cabral, et al., Carbon 146 (2019) 513–523.
[18] A.B. Dababneh, et al., J. Manuf. Sci. Eng. 136 (2014) 061016.
[19] R. Fradique, et al., J. Mater. Sci. Mater. Med. 27 (2016) 69.
[20] L. Fan, et al., Carbohydr. Polym. 146 (2016) 427–434.
[21] S.P. Miguel, et al., Carbohydr. Polym. 111 (2014) 366–373.
[22] S.M. Saraiva, et al., RSC Adv. 5 (2015) 63478–63488.
[23] S. Wang, et al., Int. J. Bioprinting (2015) 1.
[24] B.P. Antunes, et al., Carbohydr. Polym. 130 (2015) 104–112.
[25] R. Zhao, et al., Int. J. Biol. Macromol. 68 (2014) 92–97.
[26] D. Simões, et al., Eur. J. Pharm. Biopharm. 127 (2018) 130–141.
[27] X. bing Jin, et al., Biomaterials 28 (2007) 2994–3003.
[28] K.H. Bouhadir, et al., Biomaterials 22 (2001) 2625–2633.
[29] G. Diogo, et al., Biofabrication 6 (2014) 025001.
[30] E. Ruvinov, et al., Biomaterials 32 (2011) 565–578.
[31] J. Valente, et al., Mater. Sci. Eng. C 32 (2012) 2596–2603.
[32] B. Aderibigbe, et al., Pharmaceutics 10 (2018) 42.
[33] A. Khademhosseini, et al., Biomaterials 28 (2007) 5087–5092.
[34] S. Chen, et al., Nanomedicine 12 (2017) 1335–1352.
[35] Q.L. Loh, et al., Tissue Eng. Part B Rev. 19 (2013) 485–502.
[36] D. Gupta, et al., Indian J. Fibre Text. Res. (IJFTR) 39 (2014) 364–372.
[37] D.C.C. Martínez, et al., Procedia Eng. 200 (2017) 377–383.
[38] M. Tsukada, J. Appl. Polym. Sci. 22 (1978) 543–554.
[39] D. Simões, et al., React. Funct. Polym. 131 (2018) 191–202.
[40] J.J. Elsner, et al., J. Biomed. Mater. Res. Part B Appl. Biomater. 93 (2010) 425–435.
[41] M. Labet, et al., Chem. Soc. Rev. 38 (2009) 3484–3504.
[42] S.J. Hollister, Nat. Mater. 4 (2005) 518.
[43] N. Shanmugasundaram, et al., Biomaterials 22 (2001) 1943–1951.
[44] P.I. Morgado, et al., Carbohydr. Polym. 159 (2017) 136–145.
[45] Z. Li, et al., Biomaterials 26 (2005) 3919–3928.
[46] Z. Wang, et al., Sci. Rep. 4 (2014) 7064.
[47] F.-L. Mi, et al., Biomaterials 22 (2001) 165–173.
[48] P. Sudheesh Kumar, et al., ACS Appl. Mater. Interfaces 4 (2012) 2618–2629.
[49] Y. Wang, et al., Tissue Eng. Part C Methods 21 (2015) 932–944.
[50] J. Venugopal, et al., Nanotechnology 18 (2007) 055101.
[51] I. Serra, et al., Mater. Sci. Eng. C 55 (2015) 592–604.
[52] S. Zhong, et al., Wiley Interdiscip. Rev. Nanomed. Nanobiotechnol. 2 (2010) 510–525.
[53] D. Ren, et al., Carbohydr. Res. 340 (2005) 2403–2410.
[54] M.F. Jonkman, et al., Biomaterials 9 (1988) 263–267.
[55] L. Bacakova, et al., Biotechnol. Adv. 29 (2011) 739–767.
[56] S.M. Oliveira, et al., J. Adhes. Sci. Technol. 28 (2014) 843–863.
[57] K. Tsubouchi, et al., Biosci. Biotechnol. Biochem. 69 (2005) 403–405.
[58] M.P. Ribeiro, et al., Wound Repair Regen. 17 (2009) 817–824.
[59] R. Jayakumar, et al., Biotechnol. Adv. 29 (2011) 322–337.
[60] N. Kathuria, et al., Acta Biomater. 5 (2009) 406–418.
[61] S. Doakhan, et al., Carbohydr. Polym. 94 (2013) 737–748.
[62] T.T.T. Nguyen, et al., Carbohydr. Polym. 86 (2011) 1799–1806.
[63] M. Arkoun, et al., Molecules 22 (2017) 585.
[64] I. Helander, et al., Int. J. Food Microbiol. 71 (2001) 235–244.